Methanation of CO_2 over Zeolite-Encapsulated Nickel Nanoparticles

Farnoosh Goodarzi,[a] Liqun Kang,[b] Feng Ryan Wang,[b] Finn Joensen,[c] Søren Kegnæs,[a] and Jerrik Mielby[a]*

Abstract: Efficient methanation of CO_2 relies on the development of more selective and stable heterogeneous catalysts. Here we present a simple and effective method to encapsulate Ni nanoparticles in zeolite silicalite-1. In this method, the zeolite is modified by selective desilication, which creates intra-particle voids and mesopores that facilitate the formation of small and well-dispersed nanoparticles upon impregnation and reduction. TEM and XPS analysis confirm that a significant part of the Ni nanoparticles are situated inside the zeolite rather than on the outer surface. The encapsulation results in an increased metal dispersion and, consequently, a high catalytic activity for CO_2 methanation. With a gas hourly space velocity of 60000 ml/g catalyst h^{-1} and H_2/CO_2=4, the zeolite-encapsulated Ni nanoparticles result in 60% conversion at 450°C, which corresponds to a site-time yield of around 304 mol CH_4/mol Ni h^{-1}. The encapsulated Ni nanoparticles show no change in activity or selectivity after 50 h of operation, although *post*-catalysis characterisation reveals some particle migration.

Power-to-gas processes are promising strategies to store renewable energy and accommodate fluctuations in energy consumption and production.[1] In particular, much research has been devoted to the production of CH_4 by hydrogenation of CO_2,[2,3,4,5] which could be recovered from several industrial processes as well as from biogas facilities.[6] Originally discovered by Paul Sabatier in 1902,[7] the hydrogenation of CO_2 is given by the following reaction

1) $CO_2 + 4\ H_2 \rightarrow CH_4 + 2\ H_2O$

In general, it is believed that the reaction may follow two pathways. In the first pathway, CO_2 is initially converted into CO via reverse water gas shift, which is then hydrogenated into CH_4. In the second pathway, CO_2 is directly hydrogenated to CH_4 without intermediate formation of CO.[8] While several noble metals, including Ru,[9] Rh,[10] Pd,[11] Ir[12] and Pt[13] are highly active for CO_2 methanation, supported Ni nanoparticles remain the most cost-efficient catalysts.[14] Unfortunately, Ni nanoparticles are prone to sintering - a thermal deactivation caused by Ostwald ripening or particle migration and coalescence. For CO_2 methanation, which is a highly exothermic reaction operated at high temperatures, deactivation has a large impact on the process engineering. The development of more active and stable Ni catalysts could, therefore, result in considerable cost-savings in terms of the infrastructure and energy that is currently needed to cool and recycle effluent gas to prevent too high temperatures.[15] Over the years, much research has therefore been devoted to strengthen the metal-support interactions by optimising the catalyst composition.[16] Furthermore, highly stable Ni catalysts have been obtained by optimising the three-dimensional distribution of nanoparticles in ordered mesoporous materials[17, 18] or by encapsulation of nanoparticles in porous inorganic shells.[19] In particular, Laprune *et al*.[20] recently encapsulated nickel phyllosilicates in multi-hollow silicalite-1 crystals. The encapsulated nickel phyllosilicate was then reduced to Ni nanoparticles, which showed improved stability for methane steam reforming at 700°C. However, while the encapsulation was effective in keeping the encapsulated Ni nanoparticles disperse, the researchers also concluded that the catalytic activity of the encapsulated Ni nanoparticles suffered from poisoning by amorphous silica and phosphorus remaining from the synthesis. Despite of the great technological, environmental and economic interest, general methods for the encapsulation of metal nanoparticles in zeolites are still not well established. In general, the apertures of small and medium-pore zeolites preclude post-synthetic encapsulation via simple methods such as impregnation or ion-exchange,[21,22] while incorporation of metal nanoparticles during crystallization often requires expensive additives or complicated reaction procedures. Furthermore, the small apertures may also result in significant mass-transfer limitations with large and bulky substrates. While this may be exploited for interesting size-selective catalysis,[23] recent research have also focused on encapsulation of nanoparticles in zeolite with hierarchical structure or unusual morphologies that offers a reduced mean diffusion path.[24]

Building on our previous results,[25] we present here a simple and effective method to encapsulate Ni nanoparticles in zeolite silicalite-1 (S1). In this method, the zeolite is modified by selective desilication, which creates intraparticle voids and mesopores that facilitate the formation of small and disperse nanoparticles upon simple impregnation and reduction. Furthermore, we demonstrate that the catalyst with encapsulated Ni nanoparticles is significantly more active for CO_2 methanation than the corresponding catalysts prepared by impregnation of the untreated zeolite.

The selective desilication is performed in an autoclave under hydrothermal conditions using a dilute aqueous solution of ammonium hydroxide and cetyl trimethylammonium bromide (CTAB). While the ammonium hydroxide breaks poorly crystalline Si-O-Si bonds in regions inside the zeolite, the surfactant helps to protect the zeolite from the outside.[26] The desilicated zeolite (d-S1) is then calcined to remove the surfactant, dried under vacuum and impregnated with an aqueous solution of $Ni(NO_3)_2$, which fills up the internal voids and mesopores. As the material is dried and then reduced under H_2, the confined space of the zeolite framework provides ideal

[a] F. Goodarzi, Prof. S. Kegnæs, Dr. J. Mielby
DTU Chemistry
Technical University of Denmark
Kemitorvet 207, 2800 Kgs. Lyngby, Denmark
E-mail: jjmie@kemi.dtu.dk
[b] L. Kang, Dr. F. R. Wang
Department of Chemical Engineering, University College London
Torrington Place, WC1E 7JE, London, United Kingdom
[c] F. Joensen
Haldor Topsøe A/S
Haldor Topsøes Allé 1, 2800 Kgs. Lyngby, Denmark

Supporting information for this article is given via a link at the end of the document.

conditions for the preparation of small and disperse Ni nanoparticles inside the zeolite crystals. Compared to other methods,[27] this method is simple, effective and does not rely on expensive additives or complicated reaction procedures. Furthermore, the method is scalable and catalysts are easily prepared on multigram scale.

Figure 1 a shows the XRD patterns of S1, 5 wt% Ni/S1 and 5 wt% Ni/d-S1, respectively. In addition to the characteristic diffraction pattern of the MFI structured silicalite-1, the XRD pattern of Ni/S1 also shows weak diffraction peaks from Ni, while Ni/d-S1 shows weak diffraction peaks from both Ni and NiO. Since both catalysts are reduced at 500°C (see Temperature Programmed Reduction (TPR) analysis, Figure S3-4), these results show that the encapsulated Ni nanoparticles are readily re-oxidised when exposed to atmospheric air. In general, the diffraction peaks are too weak to estimate the average size of the nanoparticles by line broadening analysis.

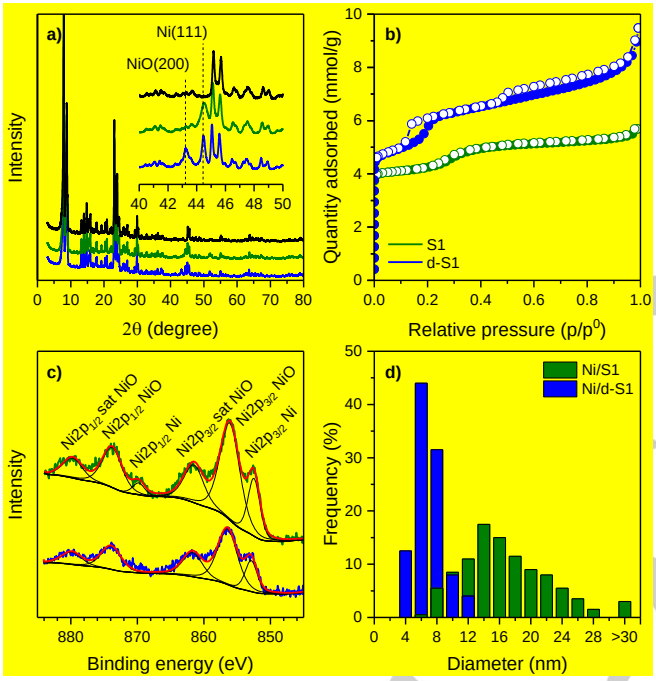

Figure 1. a) XRD analysis of parent S1 (black), Ni/S1 (green) and Ni/d-S1 (blue). b) N_2 physisorption analysis performed at 77K. c) XPS analysis of the Ni $2p_{1/2}$ and $2p_{3/2}$ level. d) Ni particle size distribution based on 200 TEM measurements.

The physisorption isotherms in Figure 1b show two typical type 1 isotherms with the exception of the small hysteresis loops at around p/p^0=0.15. These loops do not originate from mesopores, but may be explained by a fluid-to-crystal-like phase transition, which is well known for N_2 in MFI micropores.[28] Furthermore, the isotherm of Ni/d-S1 shows a significant H4 hysteresis loop that is nearly parallel at p/p^0>0.45. We assign this loop to a broad distribution of intra-particle voids and mesopores. Table 1 summarises the results from the physisorption analysis. As expected, the selective desilication results in an increased external surface area as well as an increased total pore volume, although the micropore volume is only decreased by 10%. We speculate that the selective dissolution of poorly crystalline and defect regions inside the zeolite crystals may cause this effect.

Table 1. Results from N_2 physisorption analysis at 77 K.

Support	S_{BET} $(m^2/g)^{[a]}$	S_{ext} $(m^2/g)^{[b]}$	V_{micro} $(cm_3/g)^{[b]}$	V_{tot} $(cm^3/g)^{[c]}$
S1	300	59	0.121	0.188
d-S1	367	276	0.109	0.285

[a] Calculated by the BET method. [b] Calculated by the t-plot method. [c] Determined from the isotherm adsorption branch at p/p0=0.95.

Figure 1c shows the XPS analysis of Ni/S1 and Ni/d-S1 in the Ni 2p binding energy range after reduction. The XPS spectrum of Ni/S1 show 6 clear peaks at 852.4, 856.0, 861.47, 869.6, 873,7 and 879.7 eV, respectively. We assign these peaks to the Ni $2p_{3/2}$ and Ni $2p_{1/2}$ binding energy of both Ni and NiO as well as to satellite peaks from NiO.[29] Although weaker, the same peaks also appear in the spectrum of Ni/d-S1. Since XPS is a surface sensitive analysis, the weaker intensity indicates that a significant part of the Ni nanoparticles are situated inside the zeolite. From the XPS survey spectra, we found that the fraction of Ni atoms on the surface of Ni/S1 is around 2 times higher than that on Ni/d-S1. It is noteworthy that the XPS analysis of Ni/d-S1 only show very weak peaks from $Ni(NO_3)_2$ before reduction at 500°C (see supporting information Figure S7).

The TEM images in Figure 2 give a more detailed information about the dispersion and situation of the Ni nanoparticles. While the Ni in Ni/S1 is present in the form of large and irregular agglomerates on the external surface of the zeolite, the Ni in Ni/d-S1 is present in the form of smaller and more well-defined nanoparticles primarily situated near the voids and mesoporous inside the zeolite. Although the exact three-dimensional situation of the Ni nanoparticles is difficult to determine from single TEM images, the absence of Ni nanoparticles at the edges of Ni/d-S1 crystals is typically a good indication of well-encapsulated metal nanoparticles. The size of the nanoparticles were around 8-28 nm for Ni/S1 and 4-12 nm for Ni/d-S1, see Figure 2.

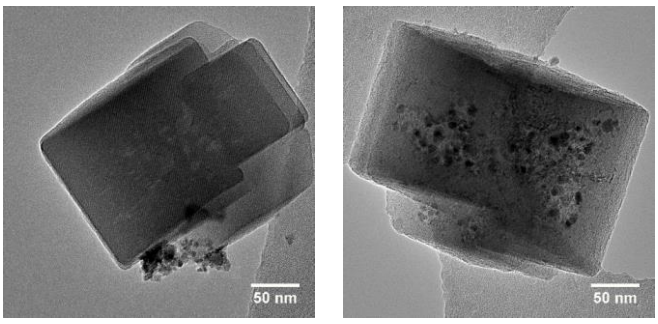

Figure 2. TEM images of Ni/S1 (left) and Ni/d-S1 (right), respectively.

Figure 3 show the Ni K edge X-ray adsorption near-edge structure (XANES) of Ni/S1 and Ni/d-S1 compared to bulk standards of NiO and Ni. The XANES spectra of the standards are consistent with those previously reported.[30] The spectra of Ni/S1 and Ni-dS1 show that the average oxidation state of the

encapsulated Ni nanoparticles in Ni/d-S1 is more similar to NiO than metallic Ni. This supports the results from XPS and XRD analysis and confirms that the small and disperse Ni nanoparticles are readily oxidised when exposed to atmospheric air. In contrast, the larger Ni nanoparticles in Ni/S1 remain more metallic in character when treated under the same conditions. The structural model derived from the analysis of the extended Ni K edge X-ray adsorption fine structure (EXAFS) spectra is fitted to Ni-O at d = 2.08 Å, Ni-Ni(1) at d = 2.48 Å and Ni-Ni(2) at d = 2.96 Å, respectively. The first nearest-neighbour shells and corresponding fitting parameters are all shown in Table S2 in the supporting information. In general, the Ni-Ni(2) scattering from Ni oxide coordination in Ni/d-S1 (C.N. = 6.8 ± 0.5) is much larger than in Ni/S1 (C.N. = 1.3 ± 0.5), while the scattering from Ni-O coordination in Ni/d-S1 (C.N. = 3.5 ± 0.5) is larger than in Ni/S1 (C.N. = 1.5 ± 0.4). Furthermore, the difference in scattering from Ni-Ni(1) coordination in Ni/S1 (C.N. = 8.2 ± 0.7) and Ni/d-S1 (C.N. = 6.1 ± 0.3) confirms that the Ni in Ni/S1 is more metallic in character.

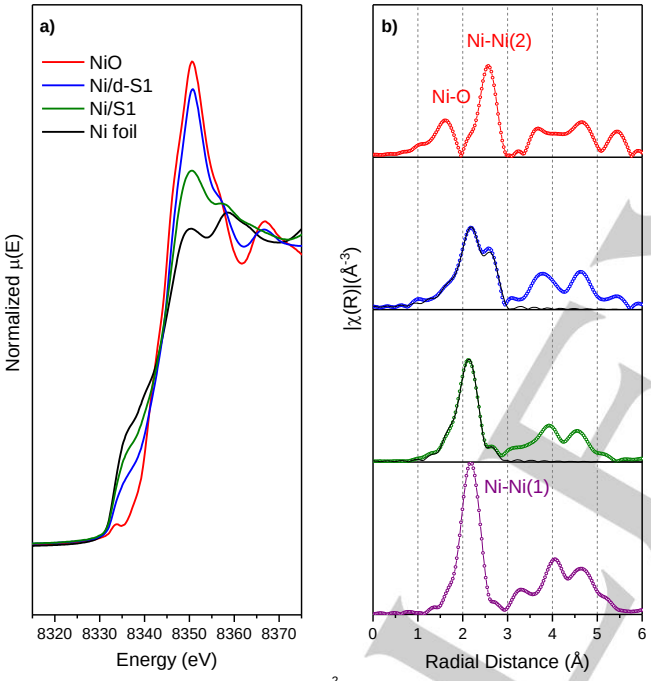

Figure 3. Ni K edge a) XANES and b) k^2-weighted R space EXAFS spectra of NiO (red), Ni/d-S1 (blue), Ni/S1 (green), Ni foil (purple), fitted results (black)

The catalytic activity for CO_2 methanation was tested in a standard fixed-bed reactor at 0.1 MPa using a ratio of H_2/CO_2=4 and a GHSV=60.000 ml/g catalyst h^{-1}. Prior to the catalytic tests, the fractionated and diluted catalyst were reduced for 2 h at 500°C under 10% H_2 in N_2.

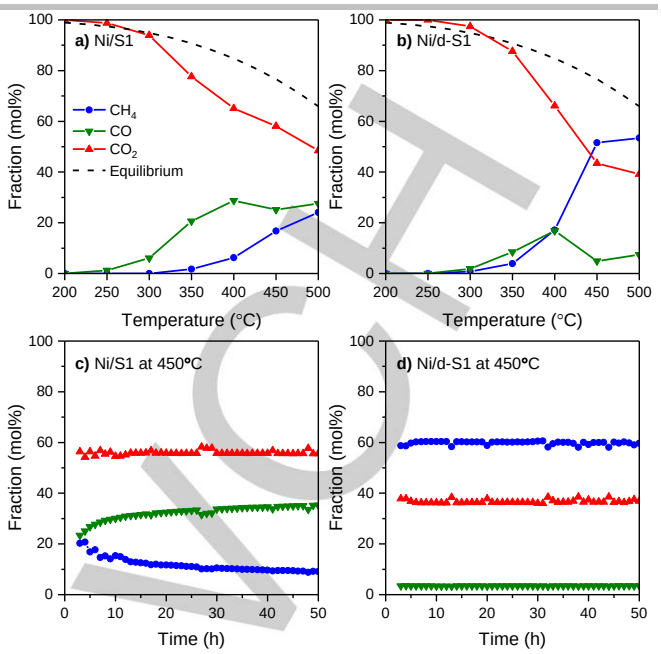

Figure 4. Molar fraction of CH_4 (blue), CO (green) and CO_2 (red) as function of the reaction temperature for a) Ni/S1 and b) Ni/d-S1. Catalytic activity over 50 h at 450°C for c) Ni/S1 and d) Ni/d-S1.

Figure 4a) and b) show the molar fraction of CH_4, CO and CO_2 as function of the temperature. No hydrocarbons other than CH_4 were detected by the online GC. In general, the catalytic activity of the Ni/S1 catalyst was relatively low. For instance, Ni/S1 only resulted in 42% conversion and 40% selectivity at 450°C, corresponding to a site time yield (STY) of around 98 mol CH_4/mol Ni h^{-1}. The catalytic activity of Ni/d-S1 was significantly higher and resulted in 57% conversion and 91% selectivity under the same conditions, corresponding to a STY of 304 mol CH_4/mol Ni h^{-1}. For comparison, Ni nanoparticles supported on USY zeolite were recently reported to have a STY of around 113 mol CH_4/mol Ni h^{-1} at a GHSV of 43000 h^{-1}.[31] The Ni/d-S1 catalysts are not only more active and selective, but also significantly more stable than Ni/S1 over time. Figure 4c) and d) show the catalytic activity of the two catalysts over 50 h at 450°C. While Ni/S1 result in a relatively stable conversion from around 42-46% over 50 h, the selectivity towards CH_4 decrease considerably from 46-21%. Under the same conditions, Ni/d-S1 results in a stable conversion of 61-64% and a selectivity of around 94-95%, which is close to the thermodynamic equilibrium. Although the catalytic activity does not appear to change over the 50 h test, TEM analysis of Ni/d-S1 after catalysis reveal some outwards migration of the nanoparticles. The particles, however, remain small and uniformly distributed (see Figure S12). In contrast, the size distribution of Ni/S1 after 50 h at 450°C is further broadened, which may be related to sintering by Ostwald ripening (see Figure S11).

In conclusion, we have developed a simple and effective method to encapsulate Ni nanoparticles in silicalite-1. The method results in a narrow size distribution of small nanoparticles that are situated inside the zeolite crystals, but remain readily accessible through the inherent microporous structure. The catalyst was demonstrated to be highly active and selective for CO_2 methanation, although the Ni nanoparticles did appear to migrate under the rough reaction conditions with both

H_2O and CO present at high temperatures. We expect that the presented method could be further improved by optimising the distribution of internal mesopores or by co-impregnation of dopants to strengthen the metal-support interactions. These approaches are therefore ongoing projects in our laboratories.

Experimental

Synthesis of Ni/S1. Tetraethyl orthosilicate (TEOS, 4.465 mL) was added dropwise to a solution of tetrapropylammonium hydroxide solution (TPAOH, 1 M, 7.265 mL) under stirring in a Teflon beaker. The mixture was stirred for 1 hour and then heated in a Teflon-lined stainless steel autoclave at 180°C for 24 h under autogenous pressure. The product was collected by filtration, washed with water, dried at room temperature and then calcined for 20 h at 550°C yielding silialite-1. After the calcination, the zeolite was dried in a vacuum oven at 50°C and then impregnated with an aqueous solution of $Ni(NO_3)_2$ to incipient wetness (5 wt% Ni loading). The impregnated zeolite was then dried at room temperature overnight and reduced under hydrogen (10% H_2 in N_2) for 2 h at 500°C.

Synthesis Ni/d-S1. Silicalite-1 (1.0 g, prepared as described above) was added to a solution of CTAB (0.7 g) in aqueous ammonia (100 mL, 3.5 wt%) and stirred for 3 h at room temperature. The solution was then transferred to a Teflon-lined stainless steel autoclave and heated to 140°C for 24 h. The product was collected by filtration, washed with water, dried overnight and then calcined at 550°C for 5 h to remove the surfactant. After the calcination, the desilicated zeolite was dried, impregnated and reduced as described above for Ni/S1.

Catalytic tests. The activity of the prepared catalysts was studied at atmospheric pressure in an microreactor setup equipped with a 5.1 mm stainless steel fixed-bed reactor, an automatic liquid-gas separator and mass flow controllers for H_2, N_2 and CO_2. The fractionated catalyst (100 mg, 180-355 µm) were diluted with fractionated quartz (600 mg, 180-355 µm) and loaded into the reactor with two pieces of quartz wool. The catalyst was then reduced for 2 h at 500°C using a heating ramp of 5°C/min and a gas composition of 5 ml H_2/min and 45 ml N_2/min. The temperature (typically 200-500°C) and gas composition (typically 80 ml/min H_2, 20 ml/min CO_2 and 20 ml/min N_2) was changed to the desired conditions and the system was allowed to equilibrate for at least 50 min before each measurement. Since no hydrocarbons other than CH_4 were detected, the gas composition was quantified from the TCD signal using the relative response factors of CO_2, CH_4 and CO, respectively. In all experiments, N_2 was used as internal standard to check the carbon balance. The experimental error was estimated from three experiments performed under standard conditions and was typically within ±5 %.

Acknowledgements

This work was funded by the Independent Research Fund Denmark (Grant no. 5054-00119 and 6111-00237) as well as by Haldor Topsøe A/S. Furthermore, the project was supported by Villum Fonden (Grant No. 13158) and the framework of EPSRC First Grant project (EP/P02467X/1) and Royal Society research grant (RG160661). We acknowledge Diamond Light Source and the UK Catalysis Hub block allocation for beamtime (SP15151) and the B18 beamline scientists for their help. The UK Catalysis Hub is kindly thanked for resources and support provided via the UK Catalysis Hub Consortium and EPSRC (portfolio grants EP/K014706/1, EP/K014668/1, EP/K014854/1, EP/K014714/1 and EP/I019693/1). Finally, we acknowledge Kristoffer Hauberg Rasmussen for help with XPS analysis.

Keywords: methanation • zeolite • encapsulated nanoparticles • nickel • heterogeneous catalysis

[1] M. Götz, J. Lefebvre, F. Mörs, A. McDaniel Koch, F. Graf, S. Bajohr, R. Reimert and T. Kolb, *Renew. Energy* **2016**, 85, 1371-1390.
[2] S. Rönsch, J. Schneider, S. Matthischke, M. Schlüter, M. Götz, J. Lefebvr, P. Prabhakaran and S. Bajohr, *Fuel* , **2016** 166, 276–296.
[3] X. Su, J. Xu, B. Liang, H. Duan, B. Hou and Y. Huang, *J. Energy Chem.* **2016**, 25, 553–565.
[4] J. Gao, Q. Liu, F. Gu, B. Liu, Z. Zhong and F. Su, *RSC Adv.* **2015**, 5, 22759-22776.
[5] W. Wei and G. Jinlong, *Front. Chem. Sci.* **2011**, 5, 2-10.
[6] P. Colleta, E. Flottes, A. Favre, L. Raynal, H. Pierre, S. Capela and C. Peregrina, *Appl. Energy* **2017**, 192, 282-295.
[7] P. Sabatier, J-B. Senderens, Comptes Rendus Des Séances De L'Académie Des Sciences, Section VI – Chimie. Paris: Imprimerie Gauthier-Villars **1902**.
[8] B. Miao, S. Su Khine Ma, X. Wang, H. Su and S. Hwa Chan, *Catal. Sci. Technol.* **2016**, 6, 4048-4058.
[9] S. Tada, O. James Ochieng, R. Kikuchi, T. Haneda, H. Kameyama, *Int. J. Hydrogen Energy* **2014**, 39, 10090-10100.
[10] A. Karelovic and P. Ruiz, *Appl. Catal. B* **2012**, 113, 237-249.
[11] J.-N. Park, E. W. McFarland, *J. Catal.* **2009**, 266, 92-97.
[12] S. Li, Y. Xu, Y. Chen, W. Li, L. Lin, M. Li, Y. Deng, X. Wang, B. Ge, C. Yang, S. Yao, J. Xie, Y. Li, X. Liu and D. Ma, *Angew. Chem.* **2017**, 56, 10761-10765.
[13] K.-P. Yu, W.-Y. Yu, M.-C. Kuo, Y.-C. Liou and S.-H. Chien, *Appl. Catal. B.* **2008**, 25, 112-118.
[14] M. A. A. Aziz, A. A. Jalil, S. Triwahyono and A. Ahmad, *Green Chem.* **2015**, 17, 2647-2663.
[15] J.R. Rostrup-Nielsen, K. Pedersen and J. Sehested, *Appl. Catal. A* **2007**, 330, 134–138.
[16] N. A. Pechimuthu , K. K. Pant, S. C. Dhingra and R. Bhalla, *Ind. Eng. Chem. Res.*, **2006**, **45**, 7435–7443.
[17] M. A. A. Aziz, A. A. Jalil, S. Triwahyono, R. R. Mukti, Y. H. Taufiq-Yap, M. R. Sazegar, *Appl. Catal. B*, **2014**, 147, 359-368.
[18] J. O. Abildstrøm, M. Kegnæs, G. Hytoft, J. Mielby and S. Kegnæs, *Micro. Meso. Mater.* **2016**, 225, 232-237.
[19] Y. Li, G. Lu and J. Ma, *RSC Adv.*, **2014**, 4, 17420-17428.
[20] D. Laprune, A. Tuel, D. Farusseng and F. C. Meunier, *ChemCatChem*, **2017**, 9, 1-12.
[21] S. Goel, S. I. Zones and E. Iglesia, *J. Am. Chem. Soc.* **2014** 136, 15280-15290.
[22] N. Wang, Q. Sun, R. Bai, X. Li, G. Guo and J. Yu, *J. Am. Chem. Soc.* **2016**, 138, 7484-7487.
[23] A. B. Laursen, K. T. Højholt, L. F. Lundegaard, S. B. Simonsen, S. Helveg. F. Schüth, M. Paul, J-D. Grunwaldt, S. Kegnæs, C. H. Christensen and K. Egeblad, *Angew. Chem.* **2010**, 49, 3504-3507.
[24] D. Farusseng and A. Tuel, *New J. Chem,* **2016**, 40, 39.

[25] J. Mielby, J. O. Abildstrøm, F. Wang, T. Kasama, C. Weidenthaler and S. Kegnæs, *Angew. Chem.*, **2014**, 126, 12721-12724.
[26] I. I. Ivanova and E. E. Knyazeva, *Chem. Soc. Rev.* **2013**, 42, 3671-3688.
[27] K. T. Højholt, A. B. Laursen, S. Kegnæs and C. H. Christensen, *Top. Catal.* **2011**, 54, 1026.
[28] P. L. Llewellyn, J.-P. Coulomb, Y. Grillet, J. Paterin, G. Andre, J. Rouquerol, *Lamgmuir*, **1993**, 9, 1846-1851.
[29] C. Zhang, L. Qian, K. Zhang, S. Yuan, J. Xiao and S. Wang, *J. Mater. Chem. A*, **2015**, 3, 10519-10525.
[30] D. J. Sprouster, R. Giulian, L. L. Araujo, P. Kluth, B. Johannesen, N. Kirby and M. C. Ridgway, *J. Appl. Phys*. **2011**, 109, 113517.
[31] M. Bacariza, I. Graça, A. Westermann, M. F. Ribeiro, J. M. Lopes and C. Henriques, *Top. Catal.* **2016**, 59, 314-325.

Entry for the Table of Contents (Please choose one layout)

Layout 1:

COMMUNICATION

Text for Table of Contents

((Insert TOC Graphic here))

*Author(s), Corresponding Author(s)**

Page No. – Page No.

Title

Layout 2:

COMMUNICATION

((Insert TOC Graphic here))

*Author(s), Corresponding Author(s)**

Page No. – Page No.

Title

Text for Table of Contents